Published in final edited form as:

Adv Mater. 2013 August 27; 25(32): 4504–4510. doi:10.1002/adma.201301656.

Fluorescent Multiblock π-Conjugated Polymer Nanoparticles for *In Vivo* Tumor Targeting

Dr. Eilaf Ahmed[+],

Department of Chemistry and Institute for Soldier Nanotechnologies, Massachusetts Institute of Technology, 77 Massachusetts Avenue, Cambridge, MA 02139 (USA)

Stephen W. Morton[+],

Department of Chemical Engineering, Massachusetts Institute of Technology, 77 Massachusetts Avenue, Cambridge, MA 02139 (USA)

Prof. Paula T. Hammond, and

Department of Chemical Engineering, Massachusetts Institute of Technology, 77 Massachusetts Avenue, Cambridge, MA 02139 (USA)

Prof. Timothy M. Swager

Department of Chemistry and Institute for Soldier Nanotechnologies, Massachusetts Institute of Technology, 77 Massachusetts Avenue, Cambridge, MA 02139 (USA)

Paula T. Hammond: hammond@mit.edu; Timothy M. Swager: tswager@mit.edu

Abstract

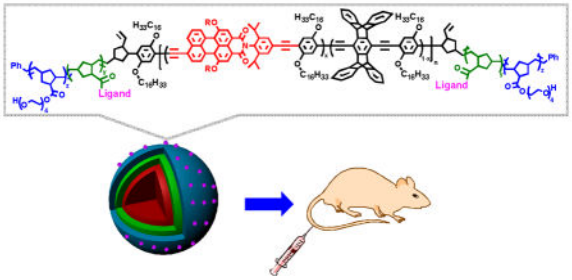

Highly fluorescent multiblock conjugated polymer nanoparticles with folic acid surface ligands are highly effective for bioimaging and *in vivo* tumor targeting. The targeted nanoparticles were preferentially localized in tumor cells *in vivo*, thereby illustrating their potential for diagnostic and therapeutic applications.

Keywords

block copolymers; conjugated polymers; nanoparticles; fluorescent bioimaging; tumor targeting

Correspondence to: Paula T. Hammond, hammond@mit.edu; Timothy M. Swager, tswager@mit.edu.

[+]These authors contributed equally to this work

((Supporting Information is available online from Wiley InterScience or from the author)).

Nanoparticle-based materials have been of significant interest for application in medical diagnostics and therapeutics.[1] New forms of nanocarriers/nanostructures for drug targeted delivery and imaging require targeting functions to recognize disease at the cellular level, a measurable readout (e.g. fluorescent tag, radiolabel) for monitoring uptake and delivery, and a therapeutic cargo.[1–2] The spectrum of nanostructured materials in this area include liposomes,[3] micelles,[4] polymer-drug conjugates,[5] dendrimers,[6] carbon nanotubes,[7] and quantum dots.[8] *In vivo* imaging and diagnostics is dominated by emissive methods and small-molecule dyes[9] and semiconductor nanocrystals[10] have emerged as the mostly widely used emissive probes for bioimaging. Materials with the most utility emit light in far-red or near-infrared (NIR) emission regions (650–1000 nm), which is characterized by minimal tissue autofluorescence and reduced scattering.[11] Several strategies have been developed to incorporate fluorescent dyes or drugs into nanostructures, including encapsulation of small-molecule dyes or covalent attachment to the particle.[12] The non-covalent encapsulation is limited by out-diffusion of the small-molecule dye, resulting in an inability to maintain complete co-localization of the fluorescent tracker with the nanostructure of interest. Furthermore, only a limited number of small-molecule dyes/or drugs can be covalently attached to the surface of the carrier system without significantly altering the carrier's physicochemical properties, such as the hydrophilicity of the polymer surface. Alternatively, covalent assembly of the dye within the nanostructures core often requires tedious synthetic efforts. Although liposomes and polymer-conjugates are among the most promising nanostructure materials for theranostics and account for the majority of clinically approved products,[1–5] there are still some drawbacks to their applications including the limited ability to encapsulate high loading of hydrophobic molecules, early burst of release of drugs, and moderate circulation half-life *in vivo* of polymer-conjugates. Thus, a new class of polymer nanostructures and modular designs that can combine a highly fluorescent probe and biomolecules for targeted therapeutic delivery using simple covalent assembly are needed to advance *in vivo* applications, particularly a platform that can allow for some degree of independent tuning of optical properties, targeting agents, and nanoparticle size.

Conjugated polymer nanoparticles (NPs)[13] are an emerging class of emissive materials for *in vivo* imaging, tumor targeting, and drug delivery.[14] Nanoparticles based on **π**-conjugated polymers are particularly attractive as a result of their high extinction coefficients, high fluorescence quantum yields, robust photostability, and the ease of functionalization with biomolecules and targeting ligands. Few classes of conjugated polymers have been studied for bioimaging including poly(*p*-phenyleneethynylene) (PPE),[15] poly(fluorene-co-phenylene),[14b, 16] and poly(benzothiadiazole)[17] and these materials have mainly been limited to *in vitro* applications. Most often, the conjugated polymers are functionalized with ionic side-chains such as carboxylate, sulfate and quaternary ammonium groups to ensure solubility in water and to facilitate interactions with biomolecules and cells.[14, 16] However, it is possible for some ionic side-chains to lead to non-specific interactions with cells and tissues. Recent *in vivo* studies using poly(benzothidadiazoles)[18] and poly(*p*-phenylenevinylene)[19] as a targeted fluorescent probe have been reported, however in these cases functionalization is achieved via less robust non-covalent surface modification.

We report herein highly fluorescent multiblock conjugated polymer nanoparticles (NPs) for bioimaging and *in vivo* tumor targeting. The conjugated polymer nanoparticles consist of a pentablock copolymer of an "ABCBA" structure, where the "C" block is a farred emitting conjugated polymer, the "A" block contains oligo(ethylene glycol)s to provide water solubility and promotes both stealth-like and an anti-fouling properties[20] needed for *in vivo* applications, and the "B" block contains reactive functionality to incorporate targeting ligands and therapeutics for tumor targeting and potentially drug payloads (Figure 1). This design is ideal for targeted drug delivery applications with a central hydrophobic to accommodate high loading of fluorescent dyes and conventional therapeutics. The outer layers consist of a hydrophilic biocompatible shell that can be functionalized with ligands/receptors for cellular recognition. Folate-receptors[21] are overexpressed on the cell membranes of many gynecologic cancer cell,[22] including ovarian cancer, thus we chose to functionalize the "B" block with folic acid to target the NPs.

Our nanoparticle designs leverage a similar pentablock copolymer structure that was used for the detection of proteases by a strain release mechanism.[23] We have similarly inserted perylene monoimide (PMI) randomly into the PPE backbone in 0.5 and 5 mol % simply by controlling the stoichiometry of the Songoshira cross-coupling polymerization. PPE-PMI copolymers were end-capped with norbornadiene[24] (NB-(PPE-PMI)-NB) to allow for further functionalization with olefin metathesis (Figure 1a). Separately, living diblock copolymers comprised of norbornene monomers with pendant oligoethyleneglycol (OEG) (A block) and *N*-hydroxysuccinate esters (NHS) (B block) were synthesized using ring opening olefin metathesis polymerization (ROMP) and then terminated by reaction with the NB-(PPE-PMI)-NB to create ABCBA-pentablock copolymers (Figure 1b). Based on ^{1}H NMR and gel permeation chromatography (GPC) the degree of polymerization for the OEG, NHS, and PPE-PMI blocks were 84, 140, and 79, respectively (Supporting Information (SI)). Finally, the OEG-NHS-(PPE-PMI)-NHS-OEG copolymers were functionalized with folic acid by attaching 20 or 50 mol % of amine terminated folate to convert the NHS esters to the corresponding amides, yielding 44 or 104 folate groups on average per polymer chain.

The polymer nanoparticles were prepared by a solvent-exchange method, wherein the conjugated polymers were initially dissolved in tetrahydrofuran (THF) or *N*,*N*-dimethylformamide (DMF) and then slowly added via syringe under sonication into a vial containing distilled water (15 mL) (Figure 1c). Absorption spectra of the NB-PPE-PMI-NB NPs in solution show peak extinction coefficients at (2.6–3.8) × 10^4 M^{-1} cm^{-1} per repeat unit (Figure S2, SI). The PL spectra display two peaks, a high-energy peak at 454 nm that can be attributed to the PPE backbone and a dominant low-energy peak which can be assigned to PMI (Figure 2a). A photograph of the NB-(PPE-PMI)-NB NPs emission under UV illumination is shown in Figure 2a (inset). Excitation of the PPE backbone at 410 nm produces a dominant emission at 604 nm from the PMI confirming efficient energy transfer in the NPs. The energy transfer efficiency can be determined by measuring the ratio of the fluorescence intensity emitted from the PMI relative to the total emission of the nanoparticles and was found to be 91 and 97% for NB-(PPE-$PMI_{0.005}$)-NB and NB-(PPE-$PMI_{0.05}$)-NB, respectively. The fluorescence quantum yields (QY) of the nanoparticles

(relative to Coumarin 6, QY= 0.78) was determined to be 0.26 and 0.14 for NB-(PPE-$PMI_{0.005}$)-NB and NB-(PPE-$PMI_{0.05}$)-NB, respectively.

We characterized the size of the NB-(PPE-PMI)-NB nanoparticles using transmission electron microscopy (TEM) and dynamic light scattering (DLS). From the TEM images shown in Figure 2b and DLS measurements (Figure S3a), it was determined that NB-(PPE-$PMI_{0.005}$)-NB NPs have a hydrodynamic diameter of 4 nm and have relatively high uniformity. The relatively high uniformity of NB-(PPE-$PMI_{0.005}$)-NB NPs can be attributed in part to filtering the NPs through a membrane filter (0.45 μm). In contrast, NPs made from NB-(PPE-$PMI_{0.05}$)-NB are relatively more polydisperse and show two populations with mean diameter of 28 and 264 nm, as seen from Figure 2c and DLS data (Figure S3b). The size of the NPs will significantly impact the pharmacokinetics[25] and cellular internalization[12] of targeted agents; as a result we endeavored to vary the size of the NPs by changing the polymer concentration in THF or DMF. Increases in the size of the NPs from 25 to 200 nm were observed, as the concentration of NB-(PPE-$PMI_{0.05}$)-NB in THF solution was increased from 50 to 200 μg/mL (Figure S4, SI). The optimum size NPs for biological applications (80–200 nm) were achieved from a polymer solution concentration of 70 μg/mL. We find that a similar concentration of OEG-NHS-(PPE-$PMI_{0.005}$)-NHS-OEG, OEG-NHS-(PPE-$PMI_{0.05}$)-NHS-OEG yields NPs in the size range of 10–200 nm (Figure S5, SI).

Folate-functionalized nanoparticles (OEG-FA-(PPE-$PMI_{0.005}$)-FA-OEG, OEG-FA-(PPE-$PMI_{0.05}$)-FA-OEG) were prepared to evaluate the binding and targeting of the conjugated polymer NPs to KB cells, which overexpress folate receptors. Live KB cells were incubated with non-functionalized (OEG-NHS-(PPE-$PMI_{0.005}$)-NHS-OEG, OEG-NHS-(PPE-$PMI_{0.05}$)-NHS-OEG) nanoparticles for 8 hours and confocal microscopy reveals (Figure 3) that folate NPs (OEG-FA-(PPE-$PMI_{0.005}$)-FA-OEG, OEG-FA-(PPE-$PMI_{0.05}$)-FA-OEG) are selectively taken up as revealed by the red fluorescence (Figure 3f). KB cells were also stained with Alexa 488 Phalloidin actin stain (Figure 3a, d) and a Hoescht nuclei stain (Figure 3b, e), which display green and blue fluorescence, respectively. Cells that were incubated with non-functionalized conjugated polymer nanoparticles (OEG-NHS-(PPE-$PMI_{0.005}$)-NHS-OEG and OEG-NHS-(PPE-$PMI_{0.05}$)-NHS-OEG) show very weak red emission, consistent with much smaller uptake of NPs (Figure 3c and Figure S6c). The enhanced cellular uptake of folate-functionalized polymer NPs is clear (Figure 3f and Figure S6f) and suggest that the NPs are internalized by KB cells. Interestingly, both the non-functionalized and functionalized particles were observed to primarily localize in the nucleus. From these data, it appears that the unique pentablock copolymers present future opportunities in gene delivery.

To examine cell-associated fluorescence, flow cytometry was used to further probe the targeting capabilities of the conjugated polymer NPs to KB cells (Figure 3g, Figures S7, S8a). After incubation of KB cells with different NP formulations for eight hours, significant associations of particles with the cells were observed for the targeted nanoparticles. Pentablock copolymers containing 5% dye (OEG-NHS-(PPE-$PMI_{0.05}$)-NHS-OEG, OEG-FA-(PPE-$PMI_{0.05}$)-FA-OEG) showed higher cell associated fluorescence compared to the one containing 0.5% dye (OEG-NHS-(PPE-$PMI_{0.005}$)-NHS-OEG, OEG-FA-(PPE-

$PMI_{0.005}$)-FA-OEG), which is due to the efficient energy transfer observed for those polymers. Internalization of folate-functionalized NPs in cancer cells appeared to be about 3 to 6-fold higher as compared to non-functionalized NPs (Figure 3g). The highest cell associated fluorescence was observed for cells incubated with the OEG-20%FA-(PPE-$PMI_{0.05}$)-20%FA-OEG. Consistent with confocal microscopy, the non-functionalized NPs also associated with the cells, however to a lesser extent, likely due to non-specific endocytotic interactions with the cell.

The inherent cytotoxicity of folate functionalized NPs (OEG-FA-(PPE-$PMI_{0.005}$)-FA-OEG, OEG-FA-(PPE-$PMI_{0.05}$)-FA-OEG) and the non-functionalized NPs (OEG-NHS-(PPE-$PMI_{0.005}$)-NHS-OEG, OEG-NHS-(PPE-$PMI_{0.05}$)-NHS-OEG) was investigated using the 3-(4,5-dimethylthiazol-2-yl)-2,5-diphenyltetrazolium bromide (MTT) viability assay. Both, the non-functionalized and functionalized NPs show negligible cytotoxicity after an incubation period of 24 to 48 h with KB cells at a concentration of 20 μg/mL (Figure 3h). Similar concentrations were consistently used for all *in vitro* and *in vivo* experiments. At higher concentrations, significant toxicity was observed only for the non-functionalized (OEG-NHS-(PPE-$PMI_{0.005}$)-NHS-OEG, OEG-NHS-(PPE-$PMI_{0.05}$)-NHS-OEG) nanoparticles, likely due to the high reactivity of NHS-ester group in aqueous medium leading to unfavorable interactions with cells (Figure S8b). The stability of the nanoparticles in serum was also investigated by temporally-resolved dynamic light scattering. Both functionalized and non-functionalized nanoparticles did not show significant change in their hydrodynamic diameter, suggesting minimum aggregation of the nanoparticles in the presence of serum (Figure S9).

The non-functionalized conjugated polymer NPs (NB-(PPE-$PMI_{0.005}$)-NB, NB-(PPE-$PMI_{0.05}$)-NB, OEG-NHS-(PPE-$PMI_{0.005}$)-NHS-OEG, OEG-NHS-(PPE-$PMI_{0.05}$)-NHS-OEG) were systemically administered into nude mice via a tail vein injection for live-animal imaging and tracking. *In vivo* fluorescence images were captured with a 3D optical imaging system (Caliper Life Sciences) up to 8 days post-injection. Figure 4 shows the NPs persist in the animal for an extended period of time, ~8 d, after which the level of quantifiable fluorescence (in units of radiant efficiency) returns to baseline autofluorescence. The extended circulation of the NPs in the animal (8 d) is remarkable particularly since most PEGylated micelle systems have moderate half-life of 2–48 h post-injection.[20, 26–27] The prolonged persistence of the NPs is expected to sufficiently facilitate their delivery to a site of interest.[28] Tissue harvesting of clearance organs, conducted 24 h post-injection, show minimal accumulation in vital organs and the majority of NPs accumulate in the GI tract and the bladder (Figure S10), consistent with the 3D optical live animal imaging (Figure 4). Together, the biodistribution, the 3D optical imaging, and tissue harvesting of the relevant organs (Figures 4, 5, S10), suggest that these nanoparticles are cleared from the body through the processes typically observed with nanoparticle systems, through the liver and via excretion. The results show that the conjugated polymer NPs traffic in the animal for a relatively long period of time with no apparent toxicity or undesirable accumulation in the animal, and underline the advantage of the NPs for targeted bioimaging and drug delivery.

We evaluated the tumor targeting strategy *in vivo* by delivering two different formulations of folate functionalized conjugated polymer NPs (OEG-50%FA-(PPE-$PMI_{0.005}$)-50%FA-OEG

and OEG-20%FA-(PPE-$PMI_{0.05}$)-20%FA-OEG) to nude mice bearing KB tumors (Figure 5a). KB xenografts were seeded in both hind flanks and allowed to grow for ~ 2 weeks until they reached approximately a size of 200 mm^3. The NPs were tail vein injected and monitored using *in vivo* imaging at an excitation of 405 nm and emission of 620 nm. Figure 5a shows the results from imaging at 24 h after injection of the NPs. Though some localization is observed, visualization of the nanoparticles by *in vivo* imaging was difficult to observe above tissue autofluorescence, likely due to the large amount of light scattered and absorbed by blood and tissue at the excitation wavelength (λ_{ex} = 405 nm). Tissue harvesting of the relevant clearance organs and tumors was conducted 24 h post-injection. The majority of the recovered fluorescence of the NPs was observed in the tumor as revealed by 3D optical imaging of harvested tissue (Figure 5b), which is also reflected in quantification of total radiant efficiency above the untreated control (for autofluorescence determination). In particular, relatively low accumulation in the liver (25%) and spleen (15%) was observed in these nanoparticle systems in comparison with PEGylated nanoparticles[27] and liposomes where accumulation in the liver can exceed 50%. The biodistribution results of the targeted NPs are also in agreement with the non-functionalized NPs, where little accumulation is observed in the liver and spleen (Figure S10). Tumor-specific accumulation was further investigated by sectioning the tumor and employing confocal microscopy to visualize NP localization in the tissue. Figure 5c shows the KB tumor morphology under optical microscopy stained with H&E stain (left) and an unstained tumor (right) section under the fluorescent microscope. The red fluorescence (λ_{ex} = 405 nm, λ_{em} = 650/50 nm) seen in an unstained tumor section (Figure 5c (right)) clearly illustrates that the folate functionalized conjugated polymer NPs accumulates effectively in the tumor, consistent with the 3D optical imaging of harvested organs. These results demonstrate that systemically-administered targeted conjugated polymer NPs were able to substantially and preferentially localize in tumor cells *in vivo*.

In conclusion, we have developed highly fluorescent multiblock conjugated polymer nanoparticles for bioimaging and *in vivo* tumor targeting. Our design utilizes simple synthetic strategies that covalently link conjugated polymers as the emissive dye and targeting moieties to create multicomponent nanostructures. We have shown that folate functionalized conjugated polymer nanoparticles exhibit significant cell-associated fluorescence *in vitro* compared to non-functionalized NPs. Further, these conjugated polymer NPs show no inherent cytotoxicity. *In vivo* studies using 3D optical imaging reveal that the NPs persist in the animal for extended periods of time with no apparent toxicity or undesirable accumulation of the NPs in the animal. We demonstrated that systemically-administered targeted conjugated polymer NPs *in vivo* can preferentially localize in tumor cells. These results clearly illustrate that our design of using multiblock copolymers is a viable approach for bioimaging and *in vivo* tumor targeting. Optimizations of the CPs core to extend the emission of the dye to far-red and NIR regions (700–900 nm) to enhance the apparent sensitivity of animal imaging to NPs (via reduced autofluorescence at the selected fluorescent channel) are underway. Further incorporation of therapeutic agents will be investigated to develop conjugated polymer NPs as a systemic delivery agent, in addition to an imaging modality.

Supplementary Material

Refer to Web version on PubMed Central for supplementary material.

Acknowledgments

This research was supported (in part) by the U.S. Army Research Office under contract W911NF-07-D-0004. We thank the Koch Institute for Integrative Cancer Research (MIT) for use of facilites. E.A. recieved postdoctoral fellowships from UNCF/Merck Science Initiative and Dr. Martin Luther King Jr. Visiting Professors and Scholars Program. S.W.M. received the National Science Foundation Graduate Research Fellowship.

References

1. a) Davis ME, Chen Z, Shin DM. Nat Rev Drug Discovery. 2008; 7:771.(b) Shi J, Votruba AR, Farokhzad OC, Langer R. Nano Lett. 2010; 10:3223. [PubMed: 20726522] c) Kievit FM, Zhang M. Adv Mater. 2011; 23:H217. [PubMed: 21842473]
2. Jain RK, Stylianopoulos T. Nat Rev Clin Oncol. 2010; 7:653. [PubMed: 20838415]
3. Torchilin VP. Nat Rev Drug Discovery. 2005; 4:145.
4. Poon Z, Chen S, Engler AC, Lee H-i, Atas E, von Maltzahn G, Bhatia SN, Hammond PT. Angew Chem. 2010; 122:7424.
5. Duncan R. Nat Rev Cancer. 2006; 6:688. [PubMed: 16900224]
6. a) Lee CC, MacKay JA, Fréchet JMJ, Szoka FC. Nat Biotech. 2005; 23:1517.b) Gillies ER, Fréchet JMJ. Drug Discovery Today. 2005; 10:35. [PubMed: 15676297] c) Amir RJ, Albertazzi L, Willis J, Khan A, Kang T, Hawker CJ. Angew Chem. 2011; 123:3487.
7. a) Yi H, Ghosh D, Ham MH, Qi J, Barone PW, Strano MS, Belcher AM. Nano Lett. 2012; 12:1176. [PubMed: 22268625] b) Robinson JT, Hong G, Liang Y, Zhang B, Yaghi OK, Dai H. J Am Chem Soc. 2012; 134:10664. [PubMed: 22667448]
8. a) Kim S, Lim YT, Soltesz EG, De Grand AM, Lee J, Nakayama A, Parker JA, Mihaljevic T, Laurence RG, Dor DM, Cohn LH, Bawendi MG, Frangioni JV. Nat Biotechnol. 2004; 22:93. [PubMed: 14661026] b) Gao X, Cui Y, Levenson RM, Chung LWK, Nie S. Nat Biotech. 2004; 22:969.
9. a) Nesterov EE, Skoch J, Hyman BT, Klunk WE, Bacskai BJ, Swager TM. Angew Chem. 2005; 117:5588.b) Gonçalves MST. Chem Rev. 2008; 109:190. [PubMed: 19105748]
10. Zrazhevskiy P, Sena M, Gao X. Chem Soc Rev. 2010; 39:4326. [PubMed: 20697629]
11. Smith AM, Mancini MC, Nie SM. Nat Nanotechnol. 2009; 4:710. [PubMed: 19898521]
12. Johnston APR, Such GK, Ng SL, Caruso F. Curr Opin Colloid Interface Sci. 2011; 16:171.
13. Pecher J, Mecking S. Chem Rev. 2010; 110:6260. [PubMed: 20684570]
14. a) Zhu C, Liu L, Yang Q, Lv F, Wang S. Chem Rev. 2012; 112:4687. [PubMed: 22670807] b) Pu KY, Liu B. Adv Funct Mater. 2011; 21:3408.
15. a) Disney MD, Zheng J, Swager TM, Seeberger PH. J Am Chem Soc. 2004; 126:13343. [PubMed: 15479090] b) Kim IB, Shin H, Garcia AJ, Bunz UHF. Bioconjugate Chem. 2007; 18:815.
16. Pu KY, Li K, Liu B. Adv Funct Mater. 2010; 20:2770.
17. Wu C, Bull B, Szymanski C, Christensen K, McNeill JD. ACS Nano. 2008; 2:2415. [PubMed: 19206410]
18. Wu C, Hansen SJ, Hou Q, Yu J, Zeigler M, Jin Y, Burnham DR, McNeill JD, Olson JM, Chiu DT. Angew Chem. 2011; 123:3492.
19. Kim S, Lim CK, Na J, Lee YD, Kim K, Choi K, Leary JF, Kwon IC. Chem Comm. 2010; 46:1617. [PubMed: 20177593]
20. Knop K, Hoogenboom R, Fischer D, Schubert US. Angew Chem. 2010; 122:6430.
21. a) Pan D, Turner JL, Wooley KL. Chem Commun. 2003:2400.b) Vlahov IR, Leamon CP. Bioconjugate Chem. 2012; 23:1357.
22. Xia W, Low PS. J Med Chem. 2010; 53:6811. [PubMed: 20666486]
23. Cordovilla C, Swager TM. J Am Chem Soc. 2012; 134:6932. [PubMed: 22489929]

24. Cox JR, Kang HA, Igarashi T, Swager TM. ACS Macro Lett. 2012; 1:334.

25. Choi HS, Liu W, Liu F, Nasr K, Misra P, Bawendi MG, Frangioni JV. Nat Nanotech. 2010; 5:42.

26. a) Huynh NT, Roger E, Lautram N, Benoit JP, Passirani C. Nanomedicine. 2010; 5:1743.b) Owens DE, Peppas NA. Int J Pharm. 2006; 307:93. [PubMed: 16303268]

27. Perry JL, Reuter KG, Kai MP, Herlihy KP, Jones SW, Luft JC, Napier M, Bear JE, DeSimone JM. Nano Lett. 2012; 12:5304. [PubMed: 22920324]

28. a) Kataoka K, Harada A, Nagasaki Y. Adv Drug Delivery Rev. 2001; 47:113.b) Alexis F, Pridgen E, Molnar LK, Farokhzad OC. Mol Pharmaceutics. 2008; 5:505.

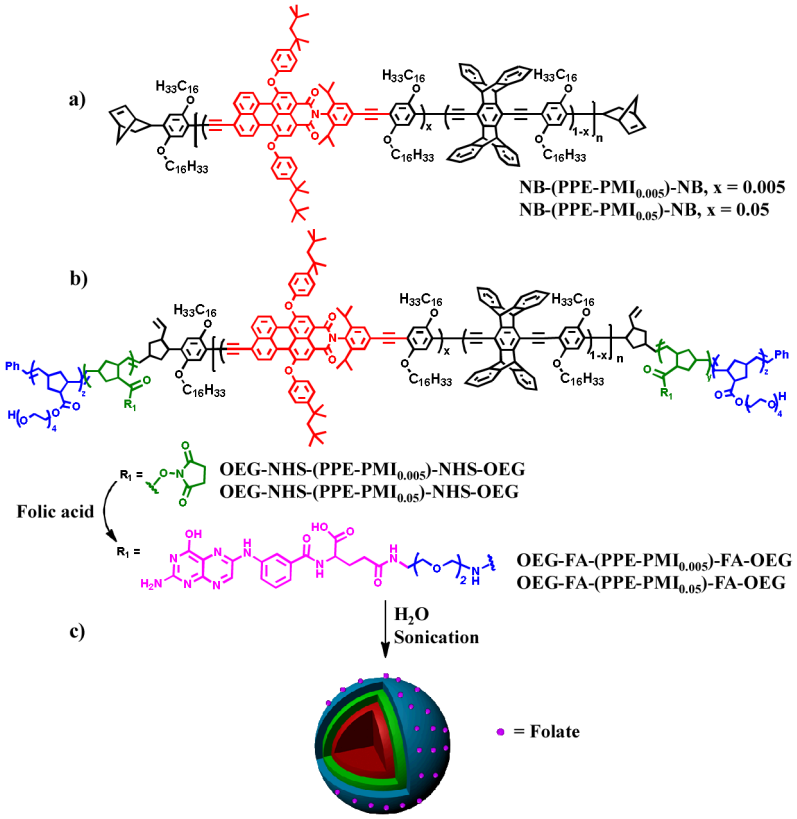

Figure 1.

Molecular structure of a) NB-(PPE-PMI)-NB, b) OEG-NHS-(PPE-PMI)-NHS-OEG and OEG-FA-(PPE-PMI)-FA-OEG, c) preparation of folate-functionalized nanoparticles.

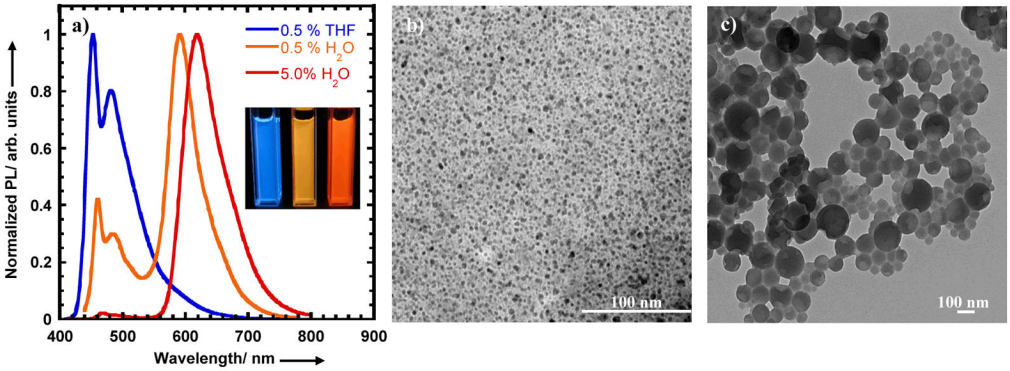

Figure 2.

a) Photoluminescene spectra of conjugated polymers in THF solution and NB-(PPE-PMI)-NB nanoparticles dispersed in water. b) A photograph of nanoparticle dispersions with different PMI/PPE ratios (mol%) under UV illumination.

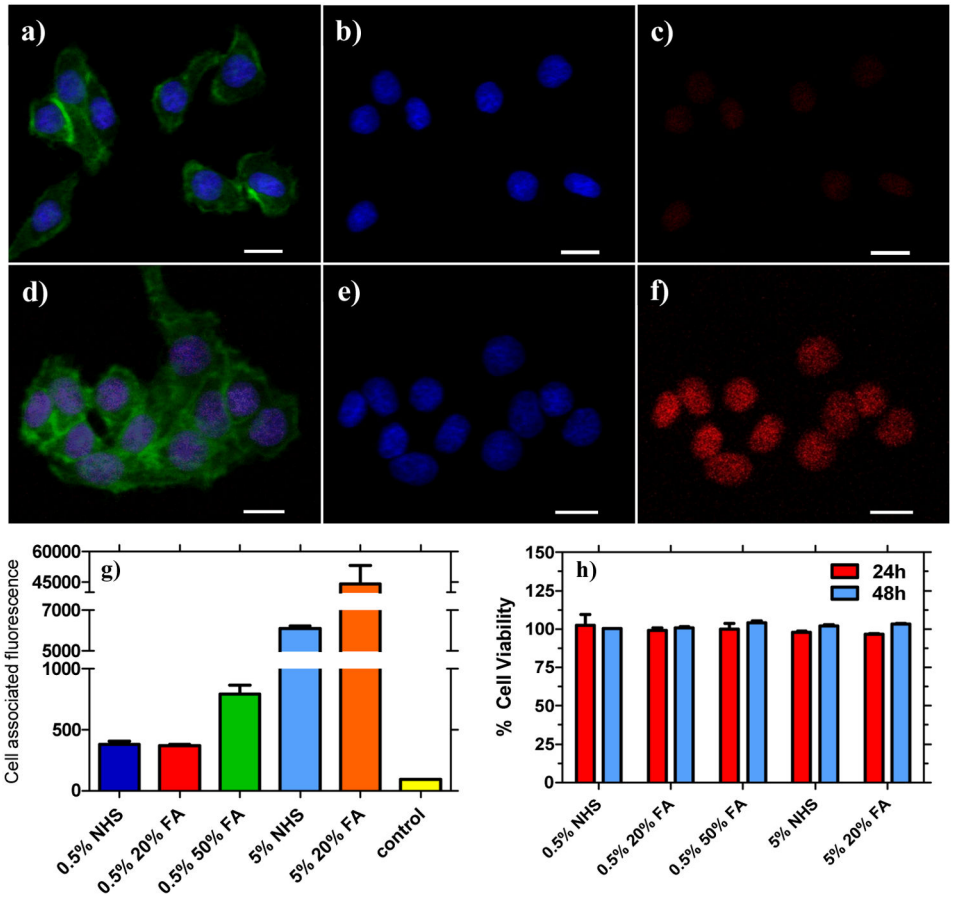

Figure 3.

Confocal microscopy images of live KB cells treated with non-functionalized (a–c) and folate-functionalized nanoparticles viewed with different filter overlays for: (a, d) stained with Alexa 488 Phalloidin actin and with Hoescht nuclei stain;; (b, e) showing only Hoescht nuclei stain; (c) nanoparticle fluorescence for OEG-NHS-(PPE-$PMI_{0.005}$)-NHS-OEG; and (f) treated with OEG-FA-(PPE-$PMI_{0.005}$)-FA-OEG. Scale bar: 20 μm. g) Measured mean cell-associated fluorescence of KB cells after 8 h. h) KB cell viability with different NPs formulation for 24 and 48 h. (0.5% NHS = OEG-NHS-(PPE-$PMI_{0.005}$)-NHS-OEG; 0.5% 20%FA = OEG-20%FA-(PPE-$PMI_{0.005}$)-20%FA-OEG; 5% NHS = OEG-NHS-(PPE-$PMI_{0.05}$)-NHS-OEG; 5% 20%FA = OEG-20%FA-(PPE-$PMI_{0.05}$)-20%FA-OEG; control = untreated KB cells).

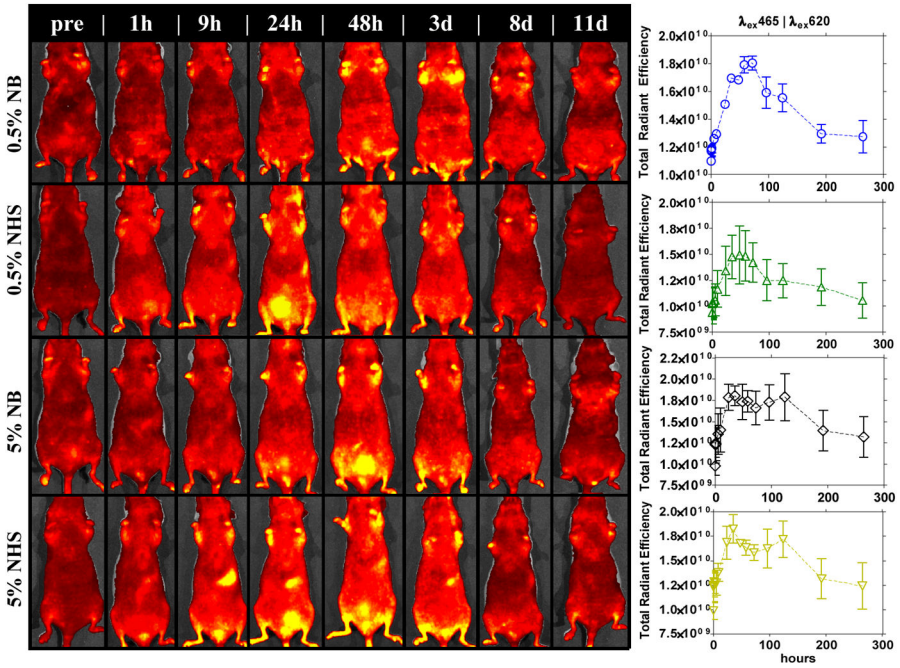

Figure 4.

Fluorescence 3D optical imaging of nude mice monitored for 10 days post-injection with different conjugated polymer NPs formulations.

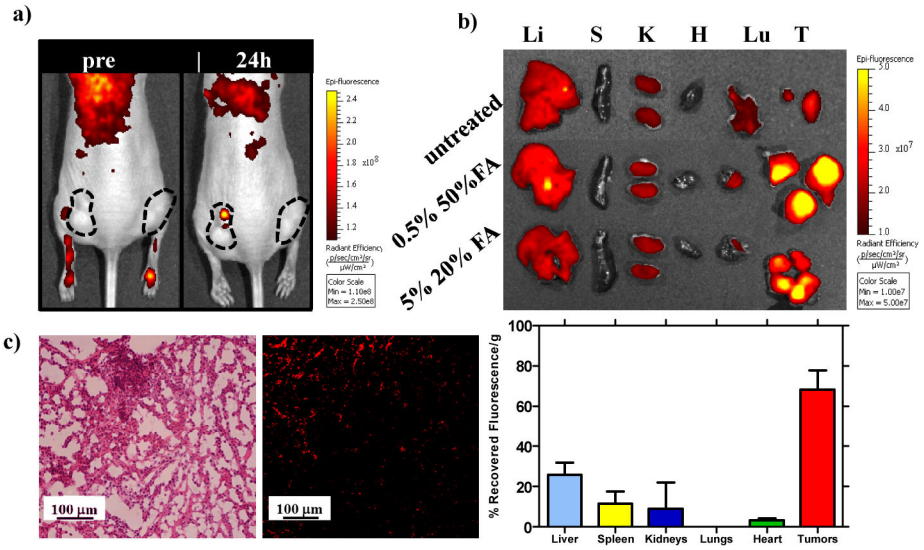

Figure 5.

a) Fluorescence 3D optical imaging of tumor-bearing nude mice at 24 h after injection with folate functionalized conjugated polymer NPs showing accumulation in tumor tissues. b) Fluorescence 3D optical imaging of harvested organs/tumors at 24 h post-injection of the functionalized NPs and recovered fluorescence in organs/tumors measured in total radiant efficiency. Confocal optical microscopy of tumor cells: c) H&E stain (left), unstained fluorescence micrograph (right) of tumor section (λ_{ex} = 405 nm, λ_{em} = 650/50 nm). Li = liver, Sp = spleen, K = kidney, Lu = lungs, H = heart, T = tumor.